Study of the torque of the bacterial flagellar motor using a rotating electric field

Jin Iwazawa, Yasuo Imae, and Syoyu Kobayasi
Department of Molecular Biology, School of Science, Nagoya University, Chikusa-ku, Nagoya, Japan 464-01

ABSTRACT Bacterial flagella are driven by a rotary motor that is energized by an electrochemical ion gradient across the cell membrane. In this study the torque generated by the flagellar motor was measured in tethered cells of a smooth-swimming *Escherichia coli* strain by using rotating electric fields to determine the relationship between the torque and speed over a wide range. By measuring the electric current applied to the sample cell and combining the data obtained at different viscosities, the torque of the flagellar motor was estimated up to 55 Hz, and also at negative rotation rates. By this method we have found that the torque of the flagellar motor linearly decreases with rotation rate from negative through positive rate of rotation. In addition, the dependence of torque upon temperature was also investigated. We showed that torque at the high speeds encountered in swimming cells had a much steeper dependence on temperature than at the low speeds encountered in tethered cells. From these results, the activation energy of the proton transfer reaction in the torque-generating unit was calculated to be about 7.0×10^{-20} J.

INTRODUCTION

E. coli has several helical flagella around its cell surface and possesses an ability to swim in aqueous medium by rotating its helical flagellar filaments as propellers. Each flagellum is rotated by a molecular rotary motor anchored in the cytoplasmic membrane (Silverman and Simon, 1974; Berg, 1974). The basal body of a flagellum embedded in the membrane is thought to serve as a rotor of the motor complex, and the stator elements and other structural components are placed around the basal body in the membrane (for recent reviews, see Blair, 1990; Jones and Aizawa, 1991).

The energy source for these motors was found to be the electrochemical potential gradient of a specific ion across the membrane; this gradient is composed of the membrane electrical potential and the chemical gradient of the ion (Manson et al., 1977; Matsuura et al., 1977; Hirota and Imae, 1983).

To understand the mechanism of energy transduction of the flagellar motor, one of the most effective methods is to investigate the mechanical properties of the motor itself. Specifically, the relationship between torque and rotation rate is a characteristic property of the motor itself, which is closely related to its mechanism. Manson et al. (1980) estimated torque at low speeds (about 10 Hz) in tethered cells of *Streptococcus*. Lowe et al. (1987) made measurements of torque at various bundle frequencies in swimming cells. Their results showed that in the case of swimming cells the torque of the motor linearly decreased with rotation rate from ~50 Hz up to 100 Hz and that values of torque of swimming cells were smaller than those of tethered cells.

In this study we attempted to measure the relationship between rate of rotation and torque of the flagellar motor in tethered cells of a smooth-swimming *E. coli* strain and determined the torque over the range 0–55 Hz speed by externally applying a rotating electric field to the cell. By this method, we were also able to extend the measurement to negative rotation (i.e., rotation in the reverse of the natural direction) up to about −20 Hz. Our measurements suggest that the torque of the flagellar motor decreases linearly with the rotation rate within the range observed. We also investigated the temperature effect on the torque versus rotation rate.

Address correspondence to Dr. Yasuo Imae, Department of Molecular Biology, School of Science, Nagoya University, Chikusa-ku, Nagoya, Japan 464-01.

PRINCIPLE

The torque M_M generated by the motor of a tethered cell rotating at angular velocity ω_O is balanced by the hydrodynamic viscous drag acting on the cell body (Fig. 1 *a*). The viscous drag may be expressed as $f\omega$ where f and ω are the frictional coefficient of the rotation of the cell about the axis through the tethering position and the angular velocity of the tethered cell, respectively.

Under an electric field, free cells migrate along the electric field by two mechanisms. One is the electrophoretic effect because the cells are carrying net charge. The other is a hydrodynamic effect due to the flow of medium driven by electroosmosis, which inevitably exists in a usual cell for the measurement of the electrophoresis (Bier, 1959). In contrast, when the same cells are tethered eccentrically on a slide glass by one of their flagella, the cells cannot migrate, but show a directional change around a tethered point by the force produced by the electrophoresis and electroosmosis.

Let us now apply an electric field rotating with an angular velocity ω_E to an eccentrically tethered cell rotating with $\omega_O (\neq \omega_E)$. Fig. 1 *b* illustrates a tethered cell rotating in the presence of an electric field at ω_E higher than its natural speed ($\omega_O < \omega_E$). Provided the electric field is sufficiently intense, the cell would be expected to rotate

0006-3495/93/03/925/09 $2.00

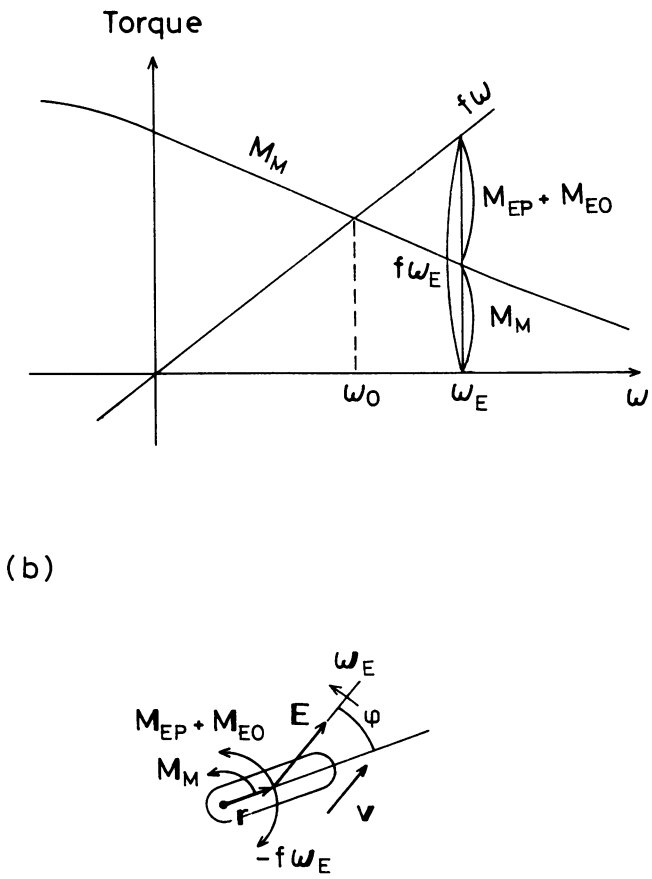

FIGURE 1 (*a*) Relationship between the torque (M_M) generated by the flagellar motor of a tethered cell and the viscous drag ($f\omega_E$) from the medium, when rotation is driven by an electrical field torque M_{EP} + M_{EO}. See the text for details. (*b*) Schematic illustration of a tethered cell which is rotated by an electric field at ω_E as described in Principle.

with ω_E, in which ϕ, the angle between the direction of the electric field and the long axis of the cell remains less than 90°.

The torque exerted on the cell body by the electrophoresis is given in terms of vectors by

$$\boldsymbol{M}_{EP} = q(\boldsymbol{r} \times \boldsymbol{E}), \tag{1}$$

or in terms of scalars by

$$M_{EP} = qrE_O \sin \phi, \quad (E_O = \|\boldsymbol{E}\|) \tag{1'}$$

where $\boldsymbol{E}$ is the rotating electric field, $\boldsymbol{r}$ is the distance from the tethering axis to the center of the cell body and q is the effective charge on the cell. In addition, a torque $\boldsymbol{M}_{EO}$ is exerted on the same cell body by the electroosmotic flow. Let us denote the velocity of the flow as $\boldsymbol{v}$, the direction of which may be parallel to the electric field. Then, the torque may be expressed in terms of vectors by

$$\boldsymbol{M}_{EO} = g(\boldsymbol{r} \times \boldsymbol{v}), \tag{2}$$

or in terms of scalars by

$$M_{EO} = grv_O \sin \phi, \quad (v_O = \|\boldsymbol{v}\|) \tag{2'}$$

where g represents a geometrical factor including the size of the cell body. Thus, the torque $\boldsymbol{M}_M$, $\boldsymbol{M}_{EP}$, $\boldsymbol{M}_{EO}$, and the hydrodynamic viscous drag on the cell body $f\omega_E$ are related by the following equation.

$$\boldsymbol{M}_M + \boldsymbol{M}_{EP} + \boldsymbol{M}_{EO} = f\omega_E, \tag{3}$$

where ω_E is the axial vector of the angular velocity of the rotating electric field. The electroosmosis is proportional to the electric field applied as described in Materials and Methods and $\boldsymbol{v}$ may be put as

$$\boldsymbol{v} = \alpha \boldsymbol{E}. \tag{4}$$

Eq. 3 equally applies to the cases of decreased speed ($0 < \omega_E < \omega_O$) and reverse rotation ($\omega_E < 0$).

Let us now gradually decrease the amplitude of the rotating electric field E_O without altering the rate ω_E. The angle ϕ will correspondingly increase toward 90° in compensation for the decline of the electric field in order to supply a constant torque, and the tethered cell will continue to rotate at the same angular velocity ω_E as the electric field. When ϕ just exceeds 90°, the synchronization is broken and rotation of the cell returns to its natural angular velocity ω_O. From Eqs. 1', 2', 3, and 4 we get the equation

$$M_M = f\omega_E - (q + g\alpha)rE_O^{90}, \tag{5}$$

where E_O^{90} is the threshold amplitude of the rotating electric field at the moment of desynchronization. According to Eq. 5, the torque of the flagellar motor at ω_E can be estimated from E_O^{90} and factors f, q, g, r, and α. However, if we use a constant-voltage mode for applying the electric field, the real values of E_O are difficult to estimate on account of the polarization at the boundary between the electrodes and the sample solution. Instead, we use the constant-current mode. Let us denote I_O as the current that passes through the sample to establish E_O in the medium. Then, the relation between E_O and I_O is written as follows:

$$E_O = kI_O/\sigma, \tag{6}$$

where k is a geometrical factor of the electrode cell and σ is the specific conductance of the sample medium. Then, substituting Eq. 6 into Eq. 5 yields

$$M_M = f\omega_E - (k/\sigma)(q + g\alpha)rI_O^{90}. \tag{7}$$

Thus, torque of the motor is represented as a linear function of both angular velocity ω_E and the threshold current I_O^{90}. When the relationship between I_O^{90} and ω_E has been obtained experimentally, the torque of the mo-

tor M_M can be expressed as a function of ω_E using Eq. 7, if the factors, f, k, q, g, r, σ, and α are known.

MATERIALS AND METHODS

Sample preparation

A smooth-swimming *Escherichia coli* strain RP4979 (*Δche Y*), whose flagellar rotation is fixed in the counterclockwise direction, was used in this study. Cells were grown to early or late logarithmic phase at 30°C with shaking in 1% tryptone (Difco Laboratories, Detroit, Michigan), 0.5% NaCl, and 0.5% glycerol (wt/vol). The cells grown in early log phase were used for observation of reverse (clockwise) rotation of tethered cells by the application of an electric field rotating in the reverse direction, because these large cells were found to be more suitable for such observations. They were harvested by centrifugation at 8,000*g* for 5 min at room temperature and washed with motility medium containing 5 mM potassium phosphate buffer (pH 7), 0.1 mM EDTA, and 0.5% glycerol, and stored on ice until use.

The viscosity of the medium was changed by addition of Ficoll 400 (Pharmacia LKB, Uppsala, Sweden) into sample medium (Manson et al., 1980). A 10% wt/vol stock solution of Ficoll 400 was prepared in motility medium. Solutions of lower Ficoll concentrations were made by dilution. Viscosity was measured in Ostwald and Ubbelohde viscometers at 25.0°C. For exchange of the motility medium, we used a modified version of the flow chamber described by Berg and Block (1984). A 3–8 min operation of a peristaltic pump type P-1 (Pharmacia Fine Chemicals, Sweden) set at a flow rate of 100–250 ml/h was sufficient for complete exchange of the content of the flow chamber.

For preparation of tethered cells, cells were sheared by passage through a Pasteur pipet (7095-5X, Corning Inc., New York) about 200 times per 1 ml medium and attached with antiflagellin antibody to an electrode cell (see below) or the bottom window of the flow chamber. Then a cover glass stored in ethanol before use was wiped with tissue and put onto the electrode cell, or the upper window of the flow chamber cleaned with ethanol and screwed into the flow chamber. These cells were allowed to incubate at room temperature for about 1 h before observation.

Measurement system

The rotation of the tethered bacterial cells was detected by an apparatus schematically shown in Fig. 2. The sample was illuminated in dark-field mode of a microscope (Nikon Co. model L equipped with 20× objective and 15× eyepiece, Tokyo, Japan) with Xenon lamp (UXL-300D, Ushio Electric Inc., Osaka, Japan). An image of the cell was focused on a linear graded filter, so that the rotation of the cell was monitored as a light signal, whose intensity was sinusoidally modulated (Kobayasi et al., 1977). The light was detected by a photomultiplier in photon counting mode with a discriminator (R649 and C1050, Hamamatsu Photonics K.K., Hamamatsu, Japan). The output of the discriminator per unit time was counted by a photon counter. Finally, these data were displayed on a personal computer (Apple II plus; Apple Computer Inc., Cupertino, California) and written on a dot printer (SP-500; Seiko Epson Co., Suwa, Japan). The rotation rates of the tethered cells were calculated from the time interval required for an integral number of cycles of the rotation. The size and shape of the cell body and the tethering position in the cell were measured by the same microscope in phase-contrast mode at the end of each measurement.

For swimming speed measurement, unsheared bacteria diluted to a suitable concentration for observation were placed in the flow chamber and observed in dark-field mode. Swimming speed was measured by analyzing the lengths of the track of the cells in the photographs (Imae et al., 1986).

To change the temperature of the medium, we placed the flow chamber filled with the sample medium on a temperature-regulated microscope stage controlled by circulation of water from a water-bath

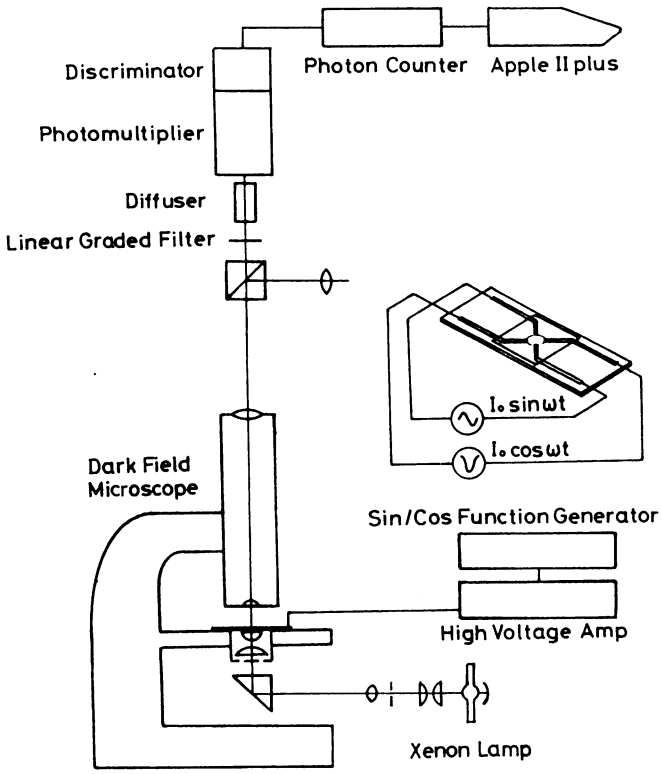

FIGURE 2 Schematic diagram of the setup for measurement of rotation rate of a tethered cell under the application of a rotating electric field through the electrode cell (*inset*). For details, see the text.

equipped with a thermostat. The temperature of the medium was measured by attaching a chromel-constantan thermocouple (0.1 mm diam.) to the frame of the flow chamber. For the calculation of torque, the temperature dependence of the viscosity of the medium was taken into account.

The electrode cell for applying a rotating electric field to tethered cells was made of a slide glass (inset of Fig. 2). Two pairs of pieces of thin platinum foil were attached around a shallow circular well (4 mm diam., 0.2 mm depth) made of epoxy resin on the glass. Sinusoidal current pulses $I_O(t) \cos \omega_E t$ and $I_O(t) \sin \omega_E t$ were then supplied to these two pairs of electrodes, where $I_O(t)$ is the amplitude of the current which was gradually decreased with time. These amplitude-modulated sinusoidal currents were generated in a home-made sine/cosine function generator and high voltage amplifier (Output max. ± 280 V). To apply the pulses in constant-current mode, resistors of 50 kΩ or 210 kΩ were connected in series between the outputs of the high voltage amplifier and the electrode cell, such that the resistance between the electrodes and the sample medium was negligible.

To test that the sum of the effects of the electrophoresis and electroosmosis is proportional to the magnitude of the applied electric field, we measured the distances of the movement of the cells by applying rectangular current pulses with a fixed duration through one pair of the electrodes of the electrode cell. Then, these distances were found to be proportional to the amplitude of the pulses in the range used in the experiments with rotating electric fields as shown in Fig. 3.

Measurement were performed at 25°C unless otherwise stated.

Calculation of frictional coefficient and torque

In order to estimate the frictional coefficient of rotating tethered cell we treated the cell body as a prolate ellipsoid and used the formula: f =

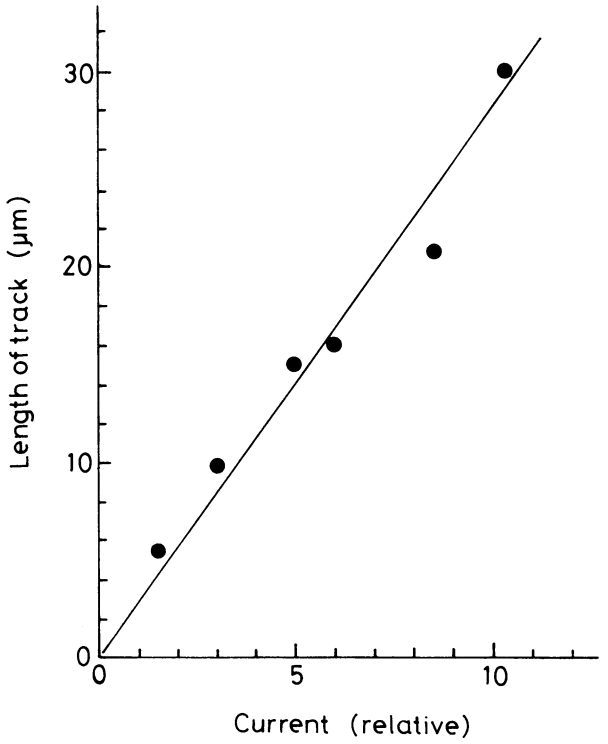

FIGURE 3 Relationship between lengths of tracks of bacterial cells and amplitude of rectangular current pulses. The pulse width is 400 ms. Flagella were sheared by passage through a Pasteur pipet. The line was drawn by eye.

$C_A^R \cos^2\theta + (C_B^R + r^2 C_B^T)\sin^2\theta$, where C_A^R and C_B^R are frictional coefficients for rotation about the major and minor axes of the prolate ellipsoid, C_B^T is the frictional coefficient for translation perpendicular to the major axis of the prolate ellipsoid, r is the distance from the tethering point of the ellipsoidal model of the cell to the center of the cell and θ is the angle between the major axis of the prolate ellipsoid and the vector ω (Sadron, 1953; Meister and Berg, 1987). The angle θ is estimated from the difference in the projected lengths of the tethered cell measured with and without a sufficient flow of the medium enough for laying down the cell parallel to the window of the flow chamber.

In case of swimming cells we calculated the torque of the motor using the formula given by Yoshida et al (1975). In application of the formula, we approximated the shape of the cell body as a prolate ellipsoid with major and minor axes of length 4.0 and 1.0 μm, and we also approximated the bundle of flagella as a helix whose wave length, amplitude, and numbers of wave were 2.24 μm, 0.22 μm, and 3, respectively. The torque calculated was divided by the mean number of 3.5 of flagella per cell so as to obtain the mean torque per motor (Yoshida et al. 1975; Lowe et al. 1987).

RESULTS

ω_E-dependence of threshold currents

We forced the rotation of tethered cells by applying an amplitude-modulated rotating electric field. Two typical examples which show a tethered cell rotating under such a field are presented in Fig. 4. Provided the electric field, which was given through current pulses, was sufficiently intense, cells rotated at the same rate as the electric field. As the electric field was gradually decreased, the synchronization was abruptly broken at some value of the current and the initial speed of the cell was immediately restored. This threshold current, I_O^{90} was determined by reading the amplitude of the current trace by eye at the moment of desynchronization from such charts as shown in Fig. 4; this current was measured several times for different rotation rates on the same cell. Results from nine cells initially rotating at about 10 Hz are plotted together in Fig. 5 *a*. Tethered cells of small size usually have a high natural speed of rotation. With these cells, however, applying an electric field for reverse rotation frequently caused the cell body to swing or vibrate and made it difficult to get reliable data for I_O^{90}. However, tethered cells of large size were easily rotated in reverse by a reverse-rotating field of up to −20 Hz. Fig. 5 *b* was constructed by using the data from 11 large cells, whose rotation rate was about 2 Hz. Both of these diagrams have positive correlations, with correlation coefficients of 0.95 and 0.96, respectively. Thus we can regard the relationship between I_O^{90} and rotation rate as a linear one. The center solid lines in the figures is a least-squares fit to the regression line

$$I_O^{90} = a + b\omega_E, \tag{8}$$

where $a = -0.257$ and $b = 4.1 \times 10^{-3}$ s in high speed cells (Fig. 5 *a*), and $a = -0.269$ and $b = 1.37 \times 10^{-2}$ s in low speed cells (Fig. 5 *b*). Upper and lower dotted lines denote 90% confidence intervals for these regression lines (Chao, 1974).

Dependence of motor torque on rotation rate

In order to get the relationship between the torque and ω_E, Eq. 8 is substituted into Eq. 7 and we get

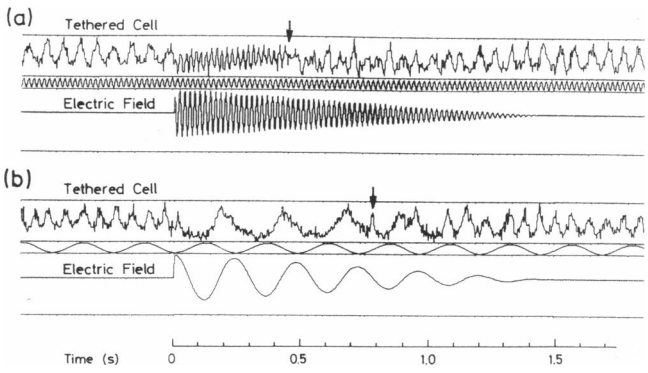

FIGURE 4 Two typical examples that represent the rotation of a tethered cell under two different rotating electric fields. The upper, middle, and lower traces correspond to the light intensity from the cell image, the time base of the rotating electric field, and the amplitude of the rotating electric field delivered in constant-current mode to the electrode cell, respectively. The natural speed $\omega_O/2\pi$ of this cell was 14.9 Hz. The arrows indicate the times at which the cell becomes unable to follow the rotation of the electric field anymore, because the amplitude of the electric field has fallen to its threshold value E_O^{90}. (*a*) $\omega_E/2\pi$ = 48.5 Hz. (*b*) $\omega_E/2\pi$ = 4.1 Hz.

$$M_M = -(ak/\sigma)(q + g\alpha)r + [f - (bk/\sigma)(q + g\alpha)r]\omega_E. \quad (9)$$

According to this equation, the torque of the motor was linearly dependent on the rotation speed within the range of our observation with the slope $f - b(k/\sigma)(q + g\alpha)r$ and the intercept $-(ak/\sigma)(q + g\alpha)r$.

To obtain the value of M_M from Eq. 9, we need the values of f, k, q, g, α, r, and σ. However, the values of k, q, g, and α are difficult to evaluate. We therefore tried to determine the slope of the line of torque versus rotation rate directly by another experimental method. We changed the natural speed of rotation of the tethered cells by changing the medium viscosity over a wide range of rotation rate in the absence of rotating electric field as described in Materials and Methods. Then motor torque can also be calculated from the hydrodynamic drag. Fig. 6 *a* shows the dependence of torque on rotation rate

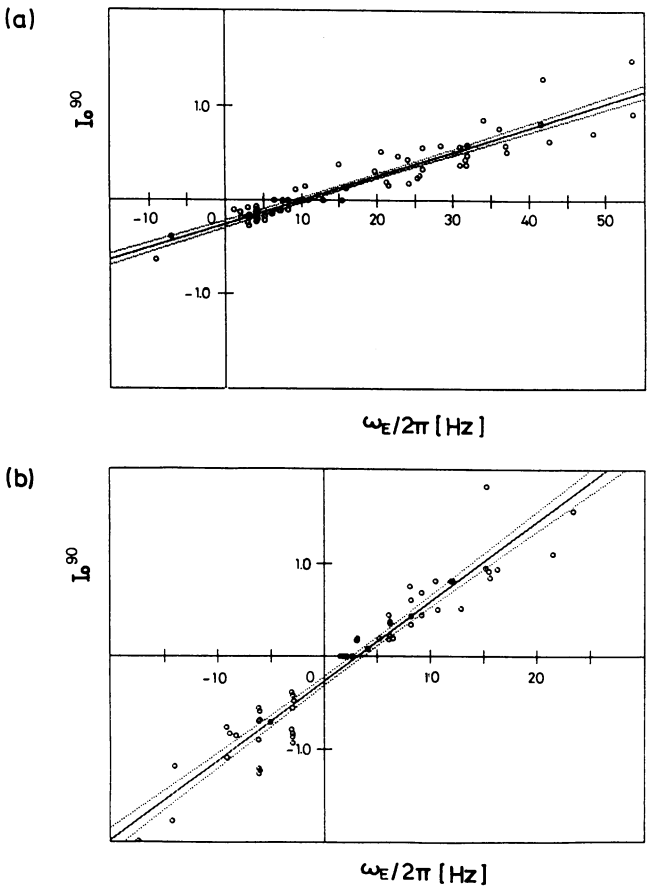

FIGURE 5 Dependence of the threshold current I_0^{90} on rotation rate of the electric field. Tethered cells of *E. coli* strain RP4979 were forced to rotate at various speeds, including reverse rotation, and the threshold currents I_0^{90} for various speeds were plotted. The scale of I_0^{90} is relative. The center solid lines are regression lines by the least-squares fit to Eq. 8 and the upper and lower dotted lines denote 90% confidence intervals for these regression lines. (*a*) Seventy datum points from nine cells that naturally rotated at nearly 10 Hz were plotted in a range from −9.1 Hz to 54 Hz. $a = -0.275$, $b = 4.1 \times 10^{-3}$ s. (*b*) Sixty-three datum points from eleven cells that naturally rotated at nearly 2 Hz were plotted in a range from −17.3 Hz to 23.4 Hz. $a = -0.269$, $b = 1.37 \times 10^{-2}$ s.

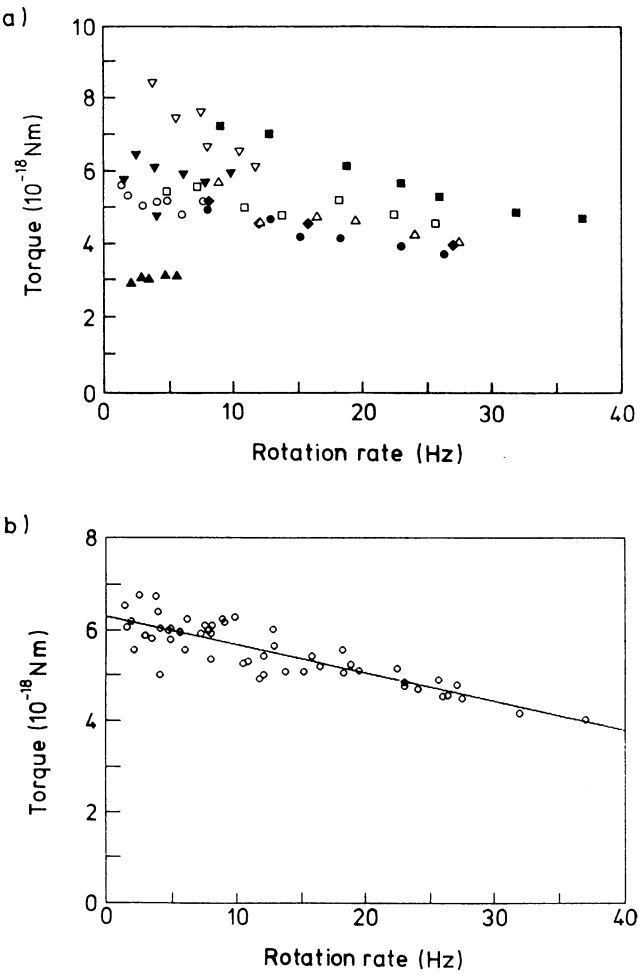

FIGURE 6 Rotation rate-dependence of torque of motors of tethered cells of *E. coli* measured by changing the medium viscosity in the absence of an electric field. (*a*) Torque of flagellar motors of *E. coli* strain RP4979 cells as a function of their natural rotation rate. Different symbols indicate different cells. The rotation rate was measured in media of various viscosities. (*b*) Normalized torques of the data in (*a*) were re-plotted together. See text for details. The regression line of Eq. 10 was calculated from the normalized data by the least-squares method. The slope and intercept are $m = -6.24 \times 10^{-20}$ Nms and $n = 6.30 \times 10^{-18}$ Nm, respectively.

obtained from nine cells. The data where the rotation rate is up to about 10 Hz were obtained from normally tethered cells ($70° < \theta < 90°$), and the data at the high speed range were obtained from the cells that were tethered in a slightly obliquely standing manner ($10° < \theta < 30°$). It is usually difficult to note such standing cells in the low viscosity regime because of their scarcity in the population and the rapidity of their rotation. In a normal medium, many cells are rotating in a visual field of the microscope; however, in high viscosity media many large cells tethered normally stop their rotation, whereas the standing cells are still rotating and are easy to detect. Although the data shown in Fig. 6 *a* are rather scattered, almost all cells exhibit a decline in motor torque with the rotation rate. Thus, these data were plotted together with

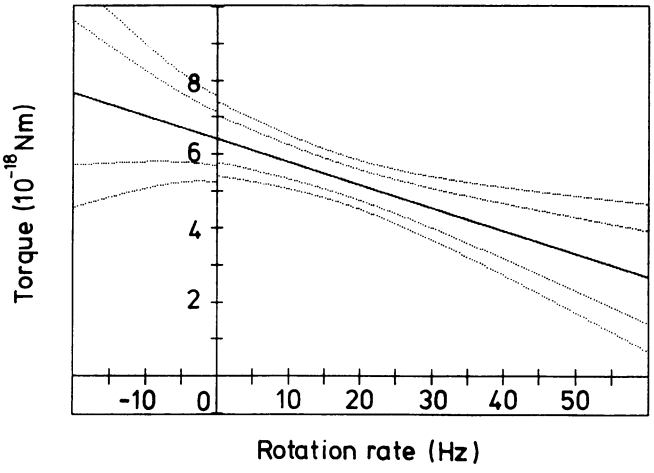

FIGURE 7 Dependence of the torque M_M on the rotation rate of the tethered cells. The center solid line corresponds to the torque of the motor calculated from Eq. 11. Outer dotted lines denote 90% confidence intervals and inner dotted lines denote 70% confidence intervals for the center line. The lines in the positive and negative regions of the rotation rate were calculated independently from the data shown in Fig. 5 *a* and in Fig. 5 *b*, respectively, and plotted together.

the stall torque of each cell normalized to be the mean value of all cells (6.3×10^{-18} Nm). The result is shown in Fig. 6 *b*. The regression line was calculated using the least-squares method and finally the torque M_M was obtained

$$M_M = n + m\omega, \tag{10}$$

where $n = 6.30 \times 10^{-18}$ Nm and $m = -6.24 \times 10^{-20}$ Nms. This equation covers speeds from 2 Hz to 38 Hz. Substituting m for $f-(bk/\sigma)(q+g\alpha)r$ in Eq. 10, we get the relation between M_M and ω_E

$$M_M = a(m-f)/b + m\omega_E. \tag{11}$$

From this equation the torque of the motor was calculated as shown in Fig. 7, where values for positive rotation rates were calculated using the parameters a and b obtained in Fig. 5 *a* and the values for negative rotation rates were calculated with the parameters obtained in Fig. 5 *b*. Similarity in the torques at $\omega = 0$ calculated from these parameters was satisfactory.

Temperature dependence of torque of the flagellar motor

We have also measured the torque of the motor at several temperatures both in tethered cells and swimming cells as shown in Table 1. The torque measured at low speeds (at high loads) are approximately 25–50 times larger than at high speeds (at low loads). As the temperature was raised, the speeds in both cases increased approximately at the constant rate with temperature. However, the torque encountered in tethered cells increased less proportionally, as compared to the torque encountered in swimming cells. Fig. 8 represents the data of Table 1 and shows the temperature dependence of the plot of torque versus speed. In the same figure, the regression line obtained at 25°C (Fig. 7) is also plotted.

TABLE 1 Effect of temperature on cell motility and torque of the motor

Temperature (°C)	Rotation rate (Hz)	Torque ($\times 10^{-18}$ Nm)
35.4	9.8	6.65
30.8	9.1	6.78
25.0	8.2	6.93
21.2	7.6	6.73
16.2	6.1	6.34
12.8	5.4	6.16
Temperature (°C)	**Swimming speed (μm/s)**	**Torque ($\times 10^{-18}$ Nm)**
35.5	44.3	0.23
31.5	38.0	0.22
27.7	32.7	0.20
23.5	27.9	0.19
19.0	22.5	0.17
14.5	17.1	0.14

Rotation rates of tethered cells were measured in medium at various temperatures (*top*) and the speeds of swimming cells were measured in the same medium at various temperatures (*bottom*). The temperature dependence of the viscosity of the medium was taken into account for the calculation of torque.

DISCUSSION

There now seems to be a consensus that torque of the flagellar motor decreases linearly with the rotation rate

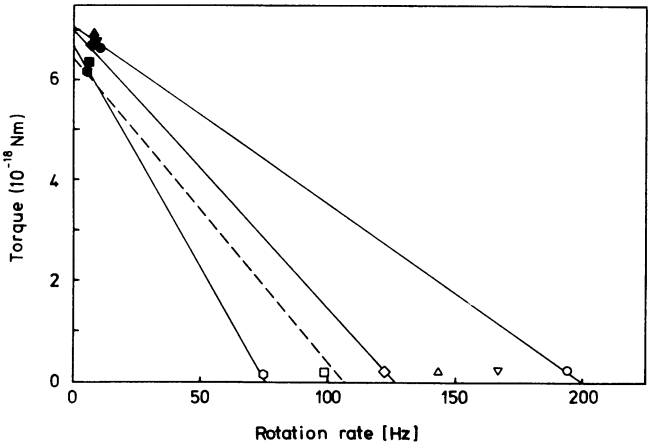

FIGURE 8 Torque of the flagellar motor of *E. coli* strain RP4979 cells as a function of the motor frequency for different values of temperature. The data were shown in Table 1. The closed symbols are derived from experiments with tethered cell at temperatures: 12.8°C (●), 16.2°C (■), 21.2°C (♦), 25.0°C (▲), 30.8°C (▼), 35.4°C (●) and the open symbols were derived from swimming cells at temperatures: 14.5°C (○), 19.0°C (□), 23.5°C (◇), 27.7°C (△), 31.5°C (▽), 35.5°C (○). The lines are to guide the eye. The dashed line corresponds to the regression line calculated from Eq. 11 as expressed in Fig. 7.

(Lowe et al., 1987; Blair, 1990). However, since measurements were performed at the low speeds encountered with tethered cells and at the high speeds encountered with swimming cells, the intermediate speed range that could not be measured, either in tethered cells or in swimming cells, remained to be estimated. Also, the torque of the motor has been measured only for the positive direction of rotation. In this study, we forced the rotation of tethered cells for not only the forward direction but also the backward direction by applying a rotating electric field, and we measured the torque of the motor from −20 Hz up to 55 Hz, including data obtained by changing medium viscosity (Figs. 5, 6, and 7). From these measurements, we have found the following three significant features of the relationship between torque and speed. (*a*) The torque of the motor linearly decreases with speed from 10 Hz to 60 Hz exactly as Lowe et al. (1987) expected. (*b*) At lower rotation rates in the range 0–10 Hz, the torque decreases with the rotation rate with the same slope as in (*a*). The drop in the torque is, however, so small (at most 10%) that the torque would have been thought to be constant in this range of the rotation rate (Manson et al., 1980). (*c*) At negative rotation rates of −20 Hz–0 Hz, we showed the result for the first time that the torque decreases linearly at the same slope as at positive rates. Thus, we concluded that the torque of the flagellar motor linearly decreases with rotation rate in the region from −20 Hz to 55 Hz.

In our system, the tethered cells were forced to rotate by a torque originated from electrophoresis as described in Principle. It is well known that the electrophoresis is accompanied by two kinds of fluid flow around the surface of the cell (Tanford, 1961). One is a bulk flow of the medium by the electroosmosis on the surface of the electrode cell, and the other is the flow of the water with ion-atmosphere in the vicinity of the bacterial cell surfaces. The latter has been corrected because we have considered the effective charge on the bacterial cell surfaces. In the case of a sphere of radius R, the effective charge, q, is given by $ZeX_1(\kappa R)/(1 + \kappa R)$, where Z, e, κ, and $X_1(x)$ are the number of charge on the sphere, elementary charge, the Debye–Hückel constant, and the Henry's function, respectively (Tanford, 1961). On the other hand, the torque arising from the medium flow by the electroosmosis has been taken into consideration as M_{EO} in Eq. 3. As for another source of torque acting on the body of the cell, a fixed dipole moment may be considered, which results from non-uniform distribution of the surface charges of bacterial cell (Adler and Shi, 1988). We rotated non-tethered cells by the rotating electric field and observed that the cells were driven in circles, keeping their directions almost fixed about their initial directions (data not shown). So under our experimental conditions, the cells can be considered to carry a very small fixed dipole moment, if any.

Although the detailed mechanism of torque generation on the flagellar motor remains almost unknown,

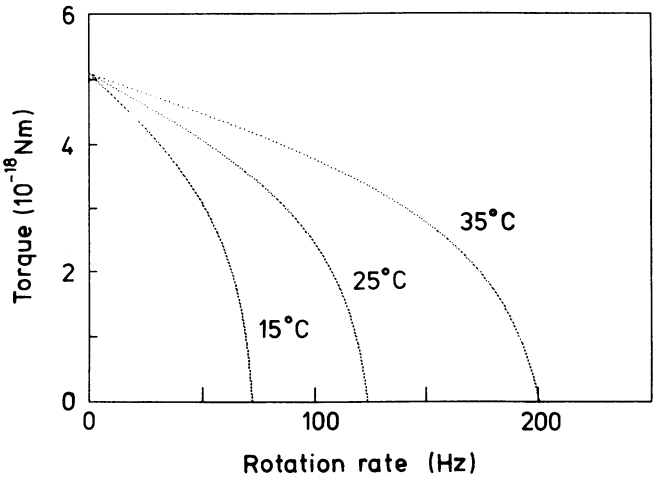

FIGURE 9 Simulations of motor torque as a function of motor frequency at different temperatures based on Appendix. The calculation has been carried out for $H_O = H_I = 10^{-7}$ M; $K_O = K_I = 10^{-7}$ M; $\Delta\phi = -200$ mV; $N = 1200$; $\Delta F^* = 7.0 \times 10^{-20}$ J.

many models have been proposed, based on various theories that involve various mechanisms of force generation. These models predicted the relation between torque and rotation rate in different ways (Oosawa and Masai, 1982; Oosawa and Hayashi, 1983; Kobayasi, 1988; Läuger, 1988; Meister et al., 1989; Murata et al., 1989; Kleutsch and Läuger, 1990). Our observations are not enough to discriminate the ideas of loose and tight coupling, because it is still unknown how the torque of the motor depends on rotation rate at very high values (Oosawa and Masai, 1982; Oosawa and Hayashi, 1983).

Torque changes only slightly with temperature at the low speeds of the tethered cells. At the high speeds of swimming cells, the torque changed noticeably with temperature as shown in Table 1, although the energy level for motor rotation, namely the proton motive force, is only slightly affected by temperature (Hirota et al., 1981). It may be assumed that the pattern of decrease of torque with rotation rate is kept on changing temperature. Therefore we have plotted torques from tethered and swimming cells together and combined these torques with lines for various temperatures as shown in Fig. 8. The regression line obtained at 25°C in Fig. 7 shows reasonable agreement with the results obtained by the experiments with different temperatures. Our observations are consistent with that obtained in *Streptococcus* (Meister et al., 1987). These temperature dependence properties may be closely connected to the mechanism of rotation of the motor. Then, we have tried to simulate the rotation rate dependence of the torque of the motor in a minimal kinetic model in order to make clear the effect of temperature upon the plot of the torque versus rotation rate (see Appendix). Typical examples of simulations are shown in Fig. 9. The results of simulations have inevitable non-linearities in the relationship between torque and rotation rate. This may be

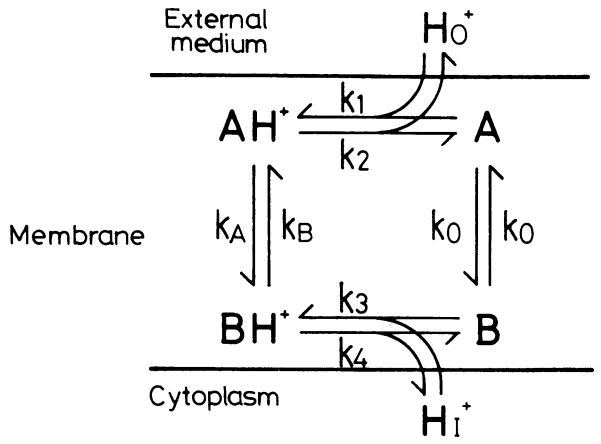

FIGURE 10 A kinetic model of transmembrane transit of protons for the flagellar motor. See text for details.

due to the simplicity of the model as described by Blair (1990). We, however, observed similar results for the simulations and the experiments as far as the temperature dependence of torque is concerned. Thus, the results of the simulation suggest further the existence of an essential rate-limiting process of proton transfer in the torque generating unit characterized with k_A and k_B as shown in Fig. 10. According to this simulation, the activation free energy ΔF^* in the reaction participating in torque generation is calculated to be 7.0×10^{-20} J.

APPENDIX

Let simplify the transmembrane transit of protons along the assembly of the flagellar motor as shown in Fig. 10. The torque is assumed to be generated from a cycling process between two states of the proton binding site in the torque generator, of which the site in state A (site A) faces the external medium and the site in state B (site B) faces the cytoplasm (Schultz, 1980). That is, when the proton in the external medium binds to site A with a bimolecular proton binding rate constant k_1, the site carrying the proton, AH^+ transits across the torque generator with a rate constant k_A and is transformed into BH^+ on the cytoplasmic side. On releasing the proton into the cytoplasm BH^+ becomes B with a rate constant k_4, and returns across the torque generator and restores the initial state A with a rate constant k_O. The reverse cycle is possible in the same manner. We assume that this process is depending on the transmembrane potential difference, in contrast with the case by Khan et al. 1990, in which two processes specified by $k_{1,2}$ and $k_{3,4}$ are depending on the transmembrane potential difference. And also we supported that, since sites A and B are non-charged carriers, the rate constant k_O for both forward and backward direction in their transmembrane transit has same value, that is given by

$$k_O = \gamma(kT/h)\exp(-\Delta F^*/kT), \qquad (A.1)$$

where k and h are the Boltzmann and Plank constants, T is the absolute temperature, γ is a geometrical factor that is usually assumed to be unity, and ΔF^* is the activation energy for the transit of the carrier across the torque generator (Zwolinski et al., 1949). Then, the steady state occupational probabilities are formulated as the following four linear equations:

$$\begin{aligned}
d[AH^+]/dt &= k_1 H_O^+[A] + k_B[BH^+] - (k_A + k_2)[AH^+] = 0,\\
d[BH^+]/dt &= k_3 H_I^+[B] + k_A[AH^+] - (k_B + k_4)[BH^+] = 0,\\
d[A]/dt &= -(k_1 H_O^+ + k_O)[A] + k_O[B] + k_2[AH^+] = 0,\\
d[B]/dt &= k_O[A] - (k_O + k_3 H_I^+)[B] + k_4[BH^+] = 0,
\end{aligned} \qquad (A.2)$$

where $k_2/k_1 = K_O$ and $k_4/k_3 = K_I$ are the dissociation constants for sites A and B, respectively, and H_O^+ and H_I^+ are the proton concentrations of the external medium and cytoplasm.

We assume that k_A and k_B participate in the torque generation without specific mechanism, where the assumption by Läuger (1988) might be considered:

$$k_A = k_O e^{-\beta} \quad \text{and} \quad k_B = k_O e^{\beta} \qquad (A.3)$$

where

$$\beta = (2\pi M/N + e\Delta\phi)/2kT, \qquad (A.4)$$

in which M is the torque generated by the unit, N is the number of protons that transit per revolution of the rotor, $\Delta\phi$ is the potential difference across the membrane, e is the elementary charge.

This system of equations together with the conservation equation

$$[A] + [B] + [AH^+] + [BH^+] = 1 \qquad (A.5)$$

allows a unique solution of the steady-state occupational probabilities of these sites by the method of elimination. The proton flux J across the motor is given by

$$\begin{aligned}
J &= k_A[AH^+] - k_B[BH^+]\\
&= k_O(K_I H_O^+ e^{-\beta} - K_O H_I^+ e^{\beta})/[2K_O K_I + K_O H_I^+ e^{\beta}\\
&\quad + K_I H_O^+ e^{-\beta} + (H_O^+ H_I^+ + k_O H_I^+/k_1 + k_O H_O^+/k_3)\\
&\quad \times (e^{-\beta} + e^{\beta}) + 2k_O(K_I e^{-\beta}/k_1 + K_O e^{\beta}/k_3)\\
&\quad + H_O^+ K_I + H_I^+ K_O].
\end{aligned} \qquad (A.6)$$

Thus, finally the rotation rate is given by

$$\omega = 2\pi J/N. \qquad (A.7)$$

We thank Y. Magariyama, S. Kudo, T. Atsumi, I. Kawagishi, and F. Oosawa for valuable suggestions and encouragement, and H. C. Berg and R. M. Macnab for valuable comments on our manuscript. We are also indebted to G. Takamatsu and S. Ishikawa of the Instrument Development Center, Faculty of Science, Nagoya University for manufacturing the optical parts of the system and the flow chamber. This work was supported in part by Grant-in-Aids to S. Kobayasi and Y. Imae from the Ministry of Education, Science and Culture of Japan.

Received for publication 27 May 1992 and in final form 24 September 1992.

REFERENCES

Adler, J., and W. Shi. 1988. Galvanotaxis in bacteria. *Cold Spring Harbor Symp. Quant. Biol.* 53:23–25.

Berg, H. C. 1974. Dynamic properties of bacterial flagellarmotors. *Nature (Lond.)*. 249:77–79.

Berg, H. C., and S. M. Block 1984. A miniature flow cell designed for rapid exchange of media under high-power microscope objectives. *J. Gen. Microbiol.* 130:2915–2920.

Bier, M. 1959. Electrophoresis, theory, methods, and applications. Academic Press Inc., Publishers, New York. p. 473.

Blair, D. F. 1990. The bacterial flagellar motor. *Sem. Cell Biol.* 1:75–85.

Chao, L. L. 1974. Statistics, Methods and Analyses. McGraw-Hill, Auckland, NZ. Chap. 14.

Hirota, N., S. Matsuura, N. Mochizuki, N. Mutoh, and Y. Imae. 1981. Use of lipophilic cation-permeable mutants for measurement of transmembrane electrical potential in metabolizing cells of *Escherichia coli*. *J. Bacteriol.* 148:399–405.

Hirota, N., and Y. Imae. 1983. Na^+-driven flagellar motors of an alkalophilic *Bacillus* strain YN-1. *J. Biol. Chem.* 258:10577–10581.

Imae, Y., H. Matsukura, and S. Kobayasi. 1986. Sodium-driven flagellar motors of alkalophilic *Bacillus*. *Methods Enzymol.* 125:582–592.

Jones, C., and S. Aizawa. 1991. The bacterial flagellum and flagellar motor: structure, assembly and function. *Adv. Microb. Physiol.* 32:109–172.

Khan, S., M. Dapice, and I. Humayan. 1990. Energy transduction in the bacterial flagellar motor: Effect of load and pH. *Biophys. J.* 57:779–796.

Kleutsch, B., and P. Läuger. 1990. Coupling of proton flow and rotation in the bacterial flagellar motor: stochastic simulation of a microscopic model. 1990. *Eur. Biophys. J.* 18:175–191.

Kobayasi, S., K. Maeda, and Y. Imae. 1977. Apparatus for detecting rate and direction of rotation of tethered bacterialcells. *Rev. Sci. Instrum.* 48:407–410.

Kobayasi, S. 1988. Diffusion motor as a model of flagellar motor of bacteria. *Ferroelectrics.* 86:335–346.

Läuger, P. 1988. Torque and rotation rate of the bacterial flagellar motor. *Biophys. J.* 53:53–65.

Lowe, G., M. Meister, and H. C. Berg. 1987. Rapid rotation of flagellar bundles in swimming bacteria. *Nature (Lond.)*. 325:637–640.

Manson, M. D., P. M. Tedesco, H. C. Berg, F. M. Harold, and C. van der Drift. 1977. A protonmotive force drives bacterial flagella. *Proc. Natl. Acad. Sci. USA.* 74:3060–3064.

Manson, M. D., P. M. Tedesco, and H. C. Berg. 1980. Energetics of flagellar rotation in bacteria. *J. Mol. Biol.* 138:541–561.

Matsuura, S., J. Shioi, and Y. Imae. 1977. Motility in *Bacillus subtilis* driven by an artificial protonmotive force. *FEBS (Fed. Eur. Biochem. Soc.) Lett.* 82:187–190.

Meister, M., and H. C. Berg. 1987. The stall torque of the bacterial flagellar motor. *Biophys. J.* 52:413–419.

Meister, M., G. Lowe, and H. C. Berg. 1987. The proton flux through the bacterial flagellar motor. *Cell.* 49:643–650.

Meister, M., S. R. Caplan, and H. C. Berg. 1989. Dynamics of a tightly coupled mechanism for flagellar rotation. *Biophys. J.* 55:905–914.

Murata, T., M. Yano, and H. Shimizu. 1989. A model of bacterial flagellar motor: free energy transduction and self-organization of rotational motion. *J. Theor. Biol.* 139:531–559.

Oosawa, F., and J. Masai. 1982. Mechanism of flagellar motor rotation in bacteria. *J. Phys. Soc. Japan.* 51:631–641.

Oosawa, F., and S. Hayashi. 1983. Coupling between flagellar motor rotation and proton flux in bacteria. *J. Phys. Soc. Japan.* 52:4019–4028.

Sadron, C. 1953. Methods of determining the form and dimensions of particles in solution: a critical survey. *Prog. Biophys.* 3:237–304.

Schultz, S. G. 1980. Basic Principles of Membrane Transport. Cambridge University Press, Cambridge, UK. Chapter 6.

Silverman, M., and M. Simon. 1974. Flagellar rotation and mechanism of bacterial motility. *Nature (Lond.)*. 249:73–74.

Tanford, C. 1961. Physical Chemistry of Macromolecules. John Wiley & Sons Inc., New York. p. 412.

Yoshida, T., K. Shimada, and S. Asakura. 1975. Cinemicrographic analysis of the movement of flagellated bacteria. I. The ratio of the propulsive velocity to the frequency of bodily rotation. *J. Mechanochem. Cell Motil.* 3:87–98.

Zwolinski B. J., H. Eyring, and C. E. Reese. 1949. Diffusion and membrane permeability. I. *J. Phys. Colloid Chem.* 53:1426–1453.